Journal of Materials Research and Technology 36 (2025) 3007–3014

Contents lists available at ScienceDirect

Journal of Materials Research and Technology

journal homepage: www.elsevier.com/locate/jmrt

Fatigue assessment and damage evolution of additively manufactured Ti–6Al–4V lattice structures for medical applications

Sebastian Stammkötter *, Selim Mrzljak, Alexander Koch, Frank Walther

Chair of Materials Test Engineering (WPT), TU Dortmund University, Baroper Str. 303, D-44227, Dortmund, Germany

ARTICLE INFO

Handling editor: L Murr

Keywords:
Ti–6Al–4V Grade 23
Lattice structures
Porous structures
fatigue behavior
additive manufacturing
Damage evolution

ABSTRACT

The possibility of patient-specific implants, using additive manufacturing, has led to a steady increase in demand, especially during the last decade. With the opportunities of layer-wise manufacturing, nearly all design and geometrical property requirements for patient-individual manufacturing can be fulfilled. Complex lattice structures, such as triply-period-minimal-surfaces (TPMS), are commonly used in medical applications to overcome problems of stress shielding. In this study, the mechanical properties and the fatigue damage evolution will be characterized using the digital image correlation (DIC) and direct current potential drop (DCPD) method. This is complemented by microstructural and computed tomography methods for a holistic characterization of the damage mechanisms and defect structure to improve the comprehension of failure mechanisms in complex lattice structures.

1. Introduction

Due to the increased strength of titanium alloys [1,2] and excellent biocompatibility [3], alloys such as Ti–6Al–4V will be used in medical implant applications [4]. Today's standard is the use of Ti–6Al–4V Grade 5 and Grade 23. These alloys show differences in content that influence mechanical, microstructural, and corrosive properties [5]. That's the reason, why Ti–6Al–4V Grade 23 is commonly used for implant applications [6,7]. The demand for personalized implants has increased significantly in recent years, as individual bone structures vary from human to human, and led to further developments regarding alloys and manufacturing processes. Additive manufacturing, especially selective laser melting (PBF-LB/M) and electron beam melting (PBF-EB/M) processes virtually eliminate production-related limitations and enable the production of complex lattice structures without design restrictions in order to reduce "stress shielding" while combining enhanced material properties and manufacturing capabilities [8,9]. Stress shielding is a cross-implant phenomenon that is caused due to the discrepancy between the implant (~110 GPa) and the human bone (~10–30 GPa) [8]. Porous structures with less density on the same volume, are called lattice structures and can be individually adapted to the requirements. Specific lattices for medical applications are typically triply-periodic-minimal-surface (TPMS), which can be used to reduce the mechanical properties such as stiffness of biomedical alloys, and increase the important prerequisite of cell adhesion after surgery for different implant applications [10–12]. As the number of additive manufacturing systems for medical fields increased rapidly, these types of implants rised up significantly and emphasized the importance of proper investigations of the mechanical properties. Consequently, the overall aim is to increase the understanding of important failure mechanisms in the context of patient safety which cannot be underestimated. In recent studies, the compressive behavior was characterized for different cell sizes and resulting densities while showing enhanced and adapted mechanical properties with reduced stiffness compared to bulk materials [13,14]. The quasistatic deformation behavior of different additively manufactured materials and lattice types was investigated using advanced measurement techniques such as digital image correlation [15,16], while the compression fatigue behavior of TPMS lattice structures was initially characterized by Hitchon et al. [17]. Furthermore, lattice structures improve energy absorption through plastic deformation and collapse of single cells/struts due to the decreased density, as well as the controllability of the corrosion behavior which are powerful and porosity-related properties for medical implant applications [18–21]. The layer-wise building strategy enables the production of complex geometries while addressing several manufacturing-related aspects such as surface roughness which

* Corresponding author.
E-mail address: sebastian.stammkoetter@tu-dortmund.de (S. Stammkötter).
URL: https://www.wpt-info.de (S. Stammkötter).

https://doi.org/10.1016/j.jmrt.2025.03.216
Received 3 February 2025; Received in revised form 24 March 2025; Accepted 24 March 2025
Available online 27 March 2025

influences the fatigue behavior and consequently the design of implants [22,23]. Therefore, further investigations focused on lattice structures while comparing these results to simulations in case of similar strain and stress accumulations to be able to predict and forecast design-relevant properties. Liu et al. [24] addressed the enhanced fatigue resistance of different cell types in the as-built condition as well as the advantages of post-processing like hot-isostatic pressing HIP to reduce manufacturing-related defects and surface roughnesses. Further studies on different lattice structures and their damage evolution were conducted by Kotzem et al. [25,26] and focused on the mechanical behavior under increased service-relevant temperatures to address and compare the deformation behavior which underlines the flexibility in application for complex lattices. As there are high requirements for the geometrical accuracy of manufacturing lattice structures with relatively high densities (~70 %), non-destructive characterization, e.g. by computed tomography is required to evaluate microporosity and surface roughness as influencing factors for the mechanical properties [27]. Further investigations [28,29] focused on the effect of microporosity in case of size, shape and morphology as well as the defect distributions on the mechanical properties of metallic components. Based on the literature on standardized unit cell-based lattice structures, further developments show adapted models and designs for medical applications. Specific designs such as Split-P TPMS lattices show improved mechanical and geometric/volumetric properties for increased tissue integration and bone regeneration of Ti–6Al–4V implants due to an even more similar structure to the human bone [30]. In addition to the advantages of the adjustment of the mechanical properties, TPMS are commonly used in the biomedical field due to their functional surface and bone-related structure which promotes important biological properties such as cell adhesion and cell growth [31].

Within this study, the local deformation behavior will be characterized using digital image correlation and the potential drop method to emphasize the complexity of measurement systems to characterize the damage mechanisms inside additively manufactured complex lattice structures including the effects of microporosity which are essential for a holistic understanding. The knowledge will be used to predict and better understand the damage mechanisms inside the human body.

2. Experimental methodology

2.1. Materials and process route

Additively manufactured Ti–6Al–4V ELI (Grade 23) specimens were processed using a TruPrint 1000 laser beam powder bed fusion (PBF-LB/M) machine by Laser Center Hannover e.V. (LZH). The PBF-LB parameters are listed in Table 1. After specimen production, additional heat treatment was conducted at 1050 °C for 4 h with subsequent oven cooling for 4 h under vacuum conditions to set an α+β microstructure (Fig. 3) without martensitic proportions.

The processed powder was produced by Eckart TLS GmbH (Bittefeld-Wolfen, Germany) with predominantly spherical morphology and particle sizes between 20.0 and 53.0 μm. The chemical composition of the powder is shown in Table 2 and was determined using an OES 720 system (Hitachi, Japan).

Specimens were designed using nTopology software (nTop, USA) to generate high-resolution stl-files for the additive manufacturing process to generate complex tensile and compression structures. The specimens are designed to focus on defined porosity (lower density on defined volume compared to bulk material) to set the required material properties for medical applications regarding stiffness to prevent stress shielding and geometrical accuracy as well as adequate surface properties to enable cell adhesion. The unit cell size (C) was chosen as 2.0 mm and is determined by $C = 2p + 2w$ whereas p is the pore size and w the wall thickness of a single unit cell. All specimens were manufactured in an upright, perpendicular position (build direction, BD), as shown in Fig. 1b.

Table 1
PBF-LB scanning parameters for Ti–6Al–4V lattice structures.

	Laser power	Scanning speed	Layer thickness	Beam diameter	Scanning rotation angle
TruPrint	140 W	1250 mm/s	30 μm	30 μm	67°

Table 2
Chemical composition of Ti–6Al–4V ELI powder.

Element	Ti	Al	V	Fe	C	Nb	Total other
wt [%]	Bal.	6.09	3.97	0.184	0.01	0.01	<0.4

2.2. Microstructural and computed tomography analyses

Microstructure analysis was performed on hot-embedded specimens, which were ground and polished up to oxide polishing suspension (OPS with colloidal SiO_2, grit size 0.3 μm). The microstructure was investigated on etched specimens (using Lichtenegger & Bloch etching suspension) under a Zeiss Axio Imager.M1m (Zeiss AG, Jena, Germany) light microscope. The Vickers hardness was determined using a DiaTester 2 (Wolpert, Germany) macro-hardness testing device (HV10) and an HMV-G (Shimadzu, Kyoto, Japan) micro-hardness testing device (HV0.01). Prior to the mechanical investigations, 3D volume scans were conducted using Nikon XT H160 and ProCon Alpha Duo computed tomography (CT) scanners, which were further analyzed regarding porosity distribution using VG StudioMax software 2024.2.1 (Volume Graphics GmbH, Heidelberg, Germany). The CT scans were evaluated regarding manufacturing defects, geometric properties, and adhesion of partially sintered, unmelted powder particles within the lattice structures. The used scan parameters were constant for all tests and are listed in Table 3.

Additional investigations regarding the macro-surface roughness of additively manufactured lattice structures were performed using an optical digital microscopy system VHX7000 (Keyence, Osaka, Japan) due to AM-specific roughness profiles. The micro-surface roughness was characterized using atomic force microscopy LightScope (NenoVision, Brno, Czech Republic) in combination with FIB-SEM investigations using a Crossbeam 550 (Zeiss AG, Jena, Germany). Further, the residual stresses before and after heat treatment were determined using a Pulstec μ-X360s with vanadium tube and 2 mm collimator.

2.3. Mechanical characterization

Quasistatic tests of TPMS lattice structures were carried out using an Instron 8801 servo-hydraulic testing system equipped with a ±100 kN load cell (Instron UK, High Wycombe, UK). A Limess Q400 3D-DIC system (Limess Messtechnik und Software GmbH, Krefeld, Germany) with 75 mm objectives and a 5 MP detector was used for (local) deformation observation and strain calculation (Fig. 2).

Further, the DIC system was used for the high cycle fatigue (HCF) investigations for monitoring of local deformation, strain, and crack evolution [32,33]. The HCF behavior was characterized using stress-controlled constant amplitude tests (CAT) at a service-relevant load ratio of $R = -1$ (fully-reversed load) and a testing frequency of $f = 10$ Hz. The damage behavior was characterized using an ImageIR 8880 thermography system (InfraTec GmbH, Dresden, Germany) and resistance measurements in the context of potential drop method. The potential drop data was recorded during the fatigue tests using QuantumX (Hottinger Bruel & Kjaer GmbH, Darmstadt, Germany) at a recording frequency of $f_R = 1000$ Hz; the current was chosen to be $I = 2.0$ A using a Soerensen XG 100–8.5 direct current source.

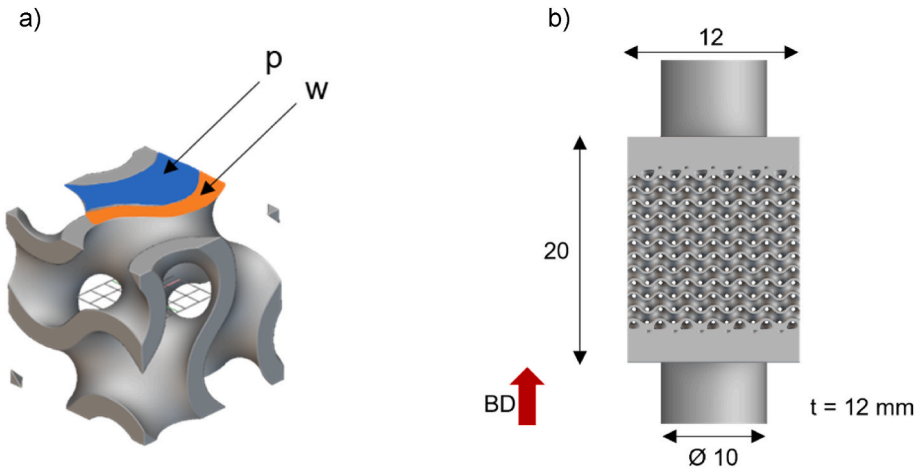

Fig. 1. a) Schematic image of TPMS unit cell; b) specimen geometry for tensile and fatigue assessment of TPMS lattice structures.

Table 3
Parameters for CT analyses of Ti–6Al–4V lattice structures.

Beam current	Beam energy	Power	Working distance	Effective pixel size	Exposure time	Exposure rate
75 µA	134 kV	10.5 W	174 mm	12.7 µm	354 ms	2.82 fps

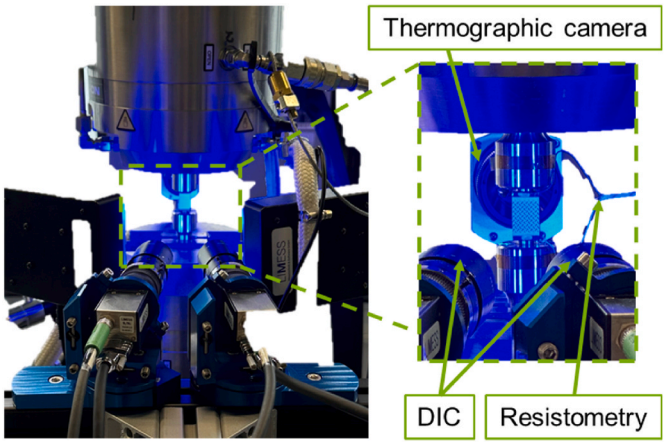

Fig. 2. Experimental setup for tensile and fatigue tests of Ti–6Al–4V lattice structures.

3. Results and discussion

3.1. Microstructure and (micro-) porosity

Prior to the mechanical characterization of the TPMS lattice structures, the microstructure of as-built (AB) and heat-treated (HT) conditions were compared in terms of grain size, distribution, and residual stresses. Scanning electron and light microscopy showed that the microstructure transformed to a homogenous α+β mixture without preferred grain orientation and increased grain size between 100 and 200 µm, highlighted in Fig. 3b and determined using the line section method. Due to stress-relief treatment after manufacturing, the measurement of the residual stresses showed that these could be reduced successfully from AB = 65 ± 9 MPa to HT = −12 ± 4 MPa.

The heat treatment led to a uniform mixed structure in all parts of the lattice. Macro- and micro-hardness measurements (Table 4) revealed no difference between solid rods and the connecting points of the lattice structures, which underlines the homogeneity of the grain distribution inside the lattice structure. The achieved Vickers hardness for both types, with a value of around 300–350 HV, is comparable to the literature [34, 35] and leads to the assumption, that the geometric structure has no influence.

Table 4
Macro- and micro-hardness of Ti–6Al–4V.

Type	Solid (PBF-LB/M)	TPMS-lattice (PBF-LB/M)
HV10	320 ± 17 HV	304 ± 4 HV
HV0.01	328 ± 21 HV	309 ± 9 HV

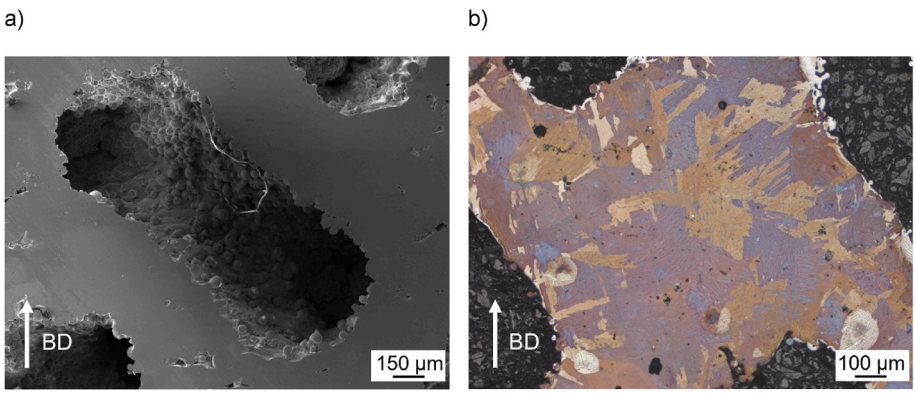

Fig. 3. a) SEM image of Ti–6Al–4V lattice structure and b) light micrograph with Ti–6Al–4V evolution in lattice.

In addition to microstructure, CT was used to analyze the manufacturing-related geometric properties and the micro-porosity of the struts. When focusing on geometric accuracy, the CT-based density calculation for the lattice part (marked in the blue rectangle in Fig. 4a) shows a global density of approx. 69.55 %, which results in an effective cross-section of approx. $A_{eff} = 100\ mm^2$. The cavities of the lattice are mostly free of powder residuals and show a homogenous shape in all areas of the structure. The inside of the structure inherits an increased surface roughness which may affect the mechanical properties. Due to lattice-specific melting strategies, there is an increased probability for micro-porosity such as gas pores and lack of fusion defects. In Fig. 4c, the defect distribution of a single specimen within a defined region of interest (see Fig. 4a) shows an enhanced number of defects with a small size and a spherical shape which leads to a higher percentage of gas porosity which results in a higher sphericity value. The equivalent defect size (dependent on real defect area and sphericity) was plotted over the number of micropores and the average sphericity factor of single defect categories. The amount of lack of fusion defects, detectable by the lower sphericity of AM components [36], is comparatively low. It is apparent, that the sphericity decreases with increasing equivalent defect size, which underlines the argumentation of a lack of fusion defects. Defects with an equivalent size of 80 μm show higher sphericity (≈0.5–0.6) than bigger defects with approx. 250–300 μm and a sphericity of 0.4. Especially the bigger defects/pores with the lower sphericity will strongly affect the mechanical properties [37,38] in combination or as well as the notch factor effect of lattices in general. Further characteristics such as perimeter, intercept and real pore are need to be taken into account due to significant effects on materials properties [39]. These factors can significantly impact the quasistatic properties as well as the fatigue lifetime and have to be carefully taken into account when focusing on fatigue failure analysis.

3.2. Quasistatic deformation behavior

The quasistatic deformation behavior of additively manufactured TPMS lattices is important to evaluate regarding the mechanical properties in the context of stiffness adaptability. Fig. 5 shows the stress-strain curves of bulk and TPMS structures to highlight the adapted mechanical properties in the context of preventing stress shielding.

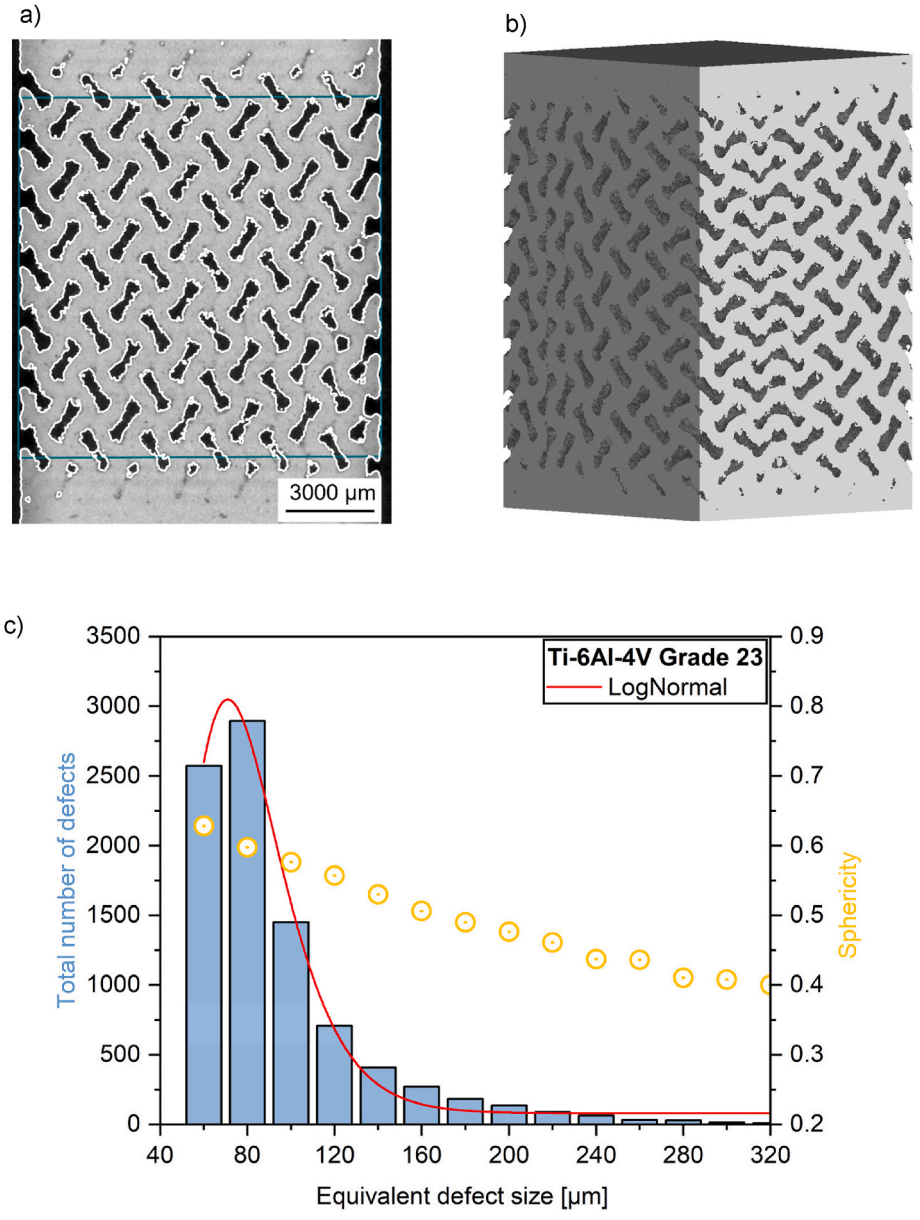

Fig. 4. a) 2D-CT side view with area of interest, b) 3D-CT reconstruction of Ti–6Al–4V lattices, and c) defect distribution with LogNormal fit and sphericity.

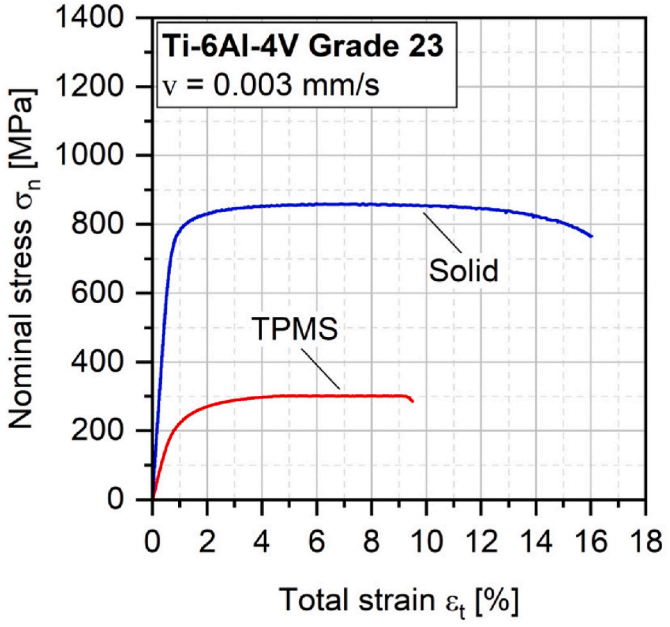

Fig. 5. Stress-strain curve of Ti–6Al–4V bulk material and lattice structure.

When comparing the tensile properties (Young's modulus (YM), yield strength (YS), ultimate tensile strength (UTS), and elongation at fracture (FS)) differences need to be properly understood for targeted use in biomedical applications. Ti–6Al–4V bulk material shows a yield strength (YS) of 784 ± 12 MPa and an ultimate tensile strength of 869 ± 7 MPa which is comparable to the literature [40]. The TPMS lattice structure shows a yield strength of 285 MPa and an ultimate tensile strength of 301 MPa which is close to factor 3 less than bulk material while reducing the mass to 69.55 % of solid. The most important parameter for implant applications is the stiffness. Due to the effective area of the TPMS lattice, the stiffness is significantly reduced from 110 to 30 GPa, reducing or preventing the phenomenon of stress-shielding [41–43]. Due to the adapted microstructure caused by the heat treatment, the ductility (FS ≈ 9 %) is high to increase the damage tolerance under cyclic loading for implant applications.

The quasistatic properties are summarized in Table 5, addressing the differences between solid and TPMS-lattice characteristics.

3.3. Fatigue behavior and damage evolution

In addition to the quasistatic performance of additively manufactured TPMS lattice structures, the fatigue behavior needs to be properly understood and characterized in terms of damage evolution and crack initiation. Fig. 6 visualizes the S–N (Woehler) curve of the TPMS lattice structure with a density of 69.55 %. The constant amplitude tests (CAT) correlate well to the Basquin equation ($R^2 = 0.98$) with a fatigue strength coefficient of $\sigma_f = 633\ MPa$ and a fatigue strength exponent of $b = -0.21$, whereas the exponent for bulk material was determined with $b = -0.12$. In addition, the scatter is low, which can be observed by analyzing the 90 % scatter band for high cycle fatigue (HCF) regime. This lattice type leads to stress amplitudes from 70 to 35 MPa within the

Table 5
Quasistatic properties of heat-treated PBF-LB/M Ti–6Al–4V. (YM: Young's modulus, YS: Yield strength, UTS: Ultimate tensile strength, FS: Fracture strain.)

	Solid (PBF-LB/M)	TPMS-lattice (PBF-LB/M)
YM (GPa)	109 ± 3	30 ± 2
YS (MPa)	784 ± 12	285 ± 4
UTS (MPa)	869 ± 7	301 ± 4
FS (%) (10-2)	16 ± 1	9 ± 1

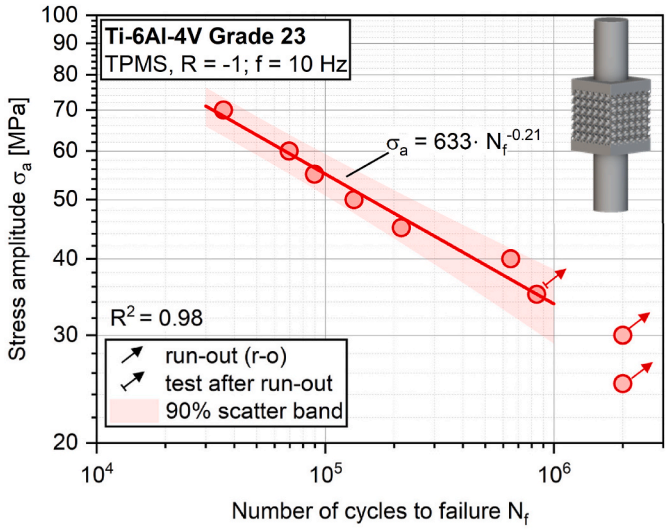

Fig. 6. S–N (Woehler) curve of Ti–6Al–4V lattice structures.

HCF regime and shows a slightly increased slope to other topic-related studies [44]. Fatigue failure was always detected in the gauge length section of the specimen. The fatigue limit was calculated to be $\sigma_f = 30 - 35\ MPa$. To include inhomogeneities of additively manufactured structures and materials, the localization of stress concentrations due to non-constant cross sections and notch effects need to be taken into account in future investigations due to influencing factors such as surface roughness, microporosity with information about shape, size, morphology and dimensions (defect distribution), and microstructure.

In addition to the fatigue strength determination, the damage mechanisms and damage evolution of the lattice structures need to be evaluated and understood to properly and safely design medical implants. Fig. 7 shows different material reactions during a fully reversed constant amplitude test of Ti–6Al–4V at a stress amplitude of $\sigma_a = 45$ MPa. Focusing on the total strain recorded using DIC, no changes can be detected up to 10^4 cycles. From 10^4 cycles up to failure, constant softening was observed, which started in regular linear decrease followed by an exponential decrease. The changes in temperature and potential show similar results with regard to the total strain up to 10^4 cycles. From this point, the recorded total strain and dynamic stiffness values show significantly increased noise which leads to the hypothesis of initial damage indications of single struts inside the structure. This is accompanied by a peakwise increase of the change in temperature curve caused by plastic deformation at the crack tip of single strut failure which needs to be validated in fractographic analyses after fatigue failure. When comparing the significance of total strain and change in potential, it can be seen that, due to the complex stress surface, the electrical resistance signal indicates a higher grade of detail and accuracy than the strain measurement. Damage inside the volume or structure cannot be fully detected/localized by optical strain measurement on the specimen's surface at the time of initial damage.

The total strain verifies the occurrence of material softening as well as the dynamic stiffness. Statements about the integral material behavior and damage indicators can reliably be detected with the used measurement instruments. The use of optical strain measurement systems is required for localized strain accumulations. This allows crack length changes and thus damage evolution to be detected and reliably analyzed on a small scale. Fig. 8a shows the change in crack length from the time of visibility on the specimen's surface as a function of the number of cycles. Due to the external trigger provided by the testing machine to the image acquisition of the DIC system, a clear assignment between individual deformation and damage images to the corresponding cycle and force signal is enabled. In addition to the change in crack length on the specimen's surface, localized strain accumulations at the gaps between

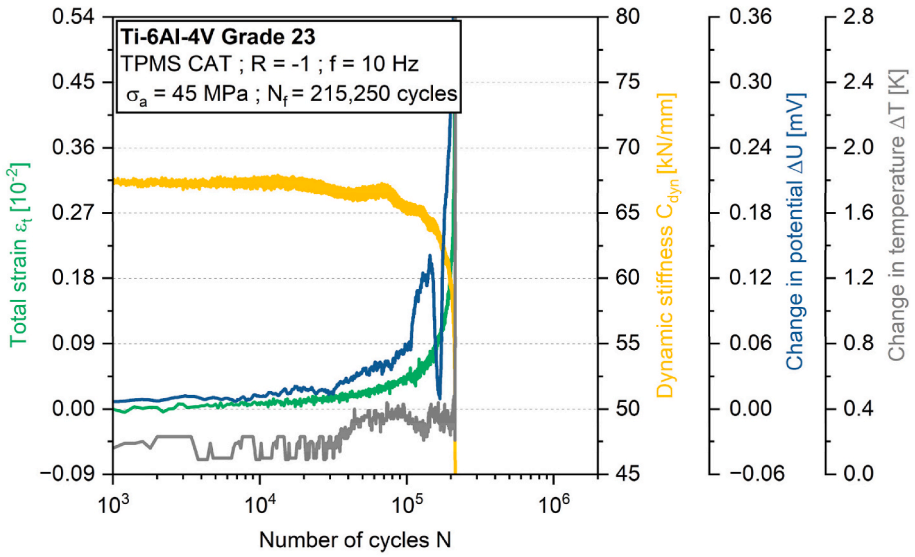

Fig. 7. Material reactions, i.e. strain, stiffness, potential, and temperature, during constant amplitude loading of Ti–6Al–4V lattice structures.

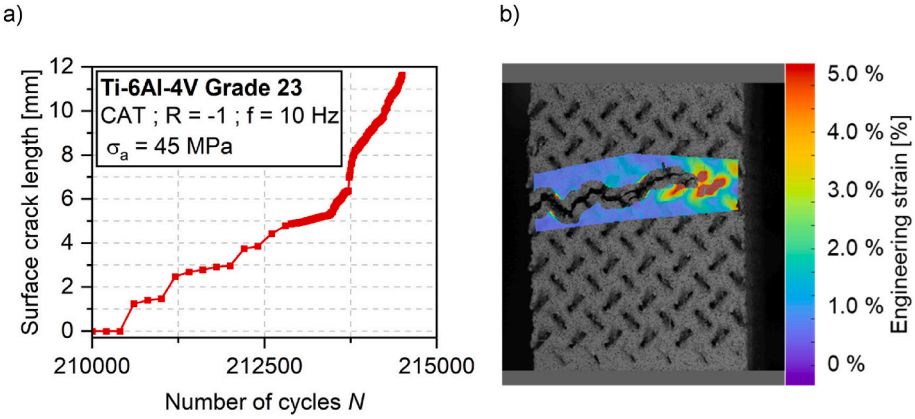

Fig. 8. Crack propagation behavior of Ti–6Al–4V lattice structures by digital image correlation (DIC): a) surface crack length versus number of cycles and b) visualized crack detection.

the struts can be observed using optical strain measurement, which is impossible by classic tactile measuring instruments. This allows notch factors and other information to be obtained from the optically generated data. The images show that crack propagation is stable up to around $2.13 \cdot 10^5$ cycles and changes to exponential crack growth with residual force fracture only shortly before final failure.

Focusing on the fractographic analysis presented in Fig. 9, illustrating the fracture surface in Fig. 9a of a fatigue specimen subjected to a stress amplitude of 45 MPa, the crack initiation area (Fig. 9b) was carefully determined using scanning electron microscopy (SEM). The analysis revealed a significant presence of unmelted powder particles from the additive manufacturing process. These particles contribute to crack initiation, predominantly observed at sharp notches along the lattice structure surface. Furthermore, the fractographic observations indicate a consistent and uniform crack propagation confined within the same plane of the lattice structure.

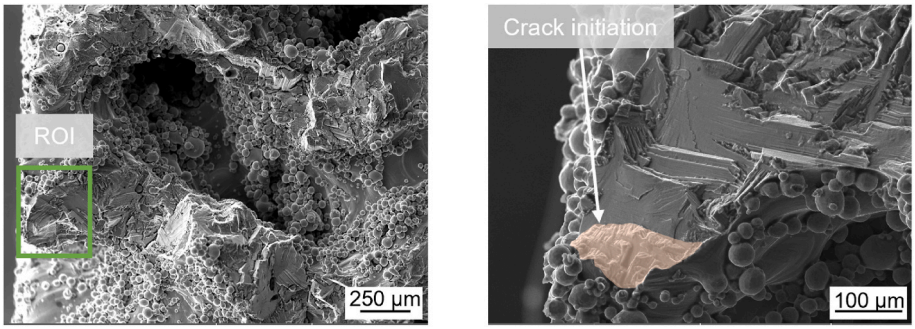

Fig. 9. a) Fractography of Ti–6Al–4V lattice structures after constant amplitude loading with stress amplitude of $\sigma_a = 45$ MPa and b) SEM micrograph of the region of interest with high magnification.

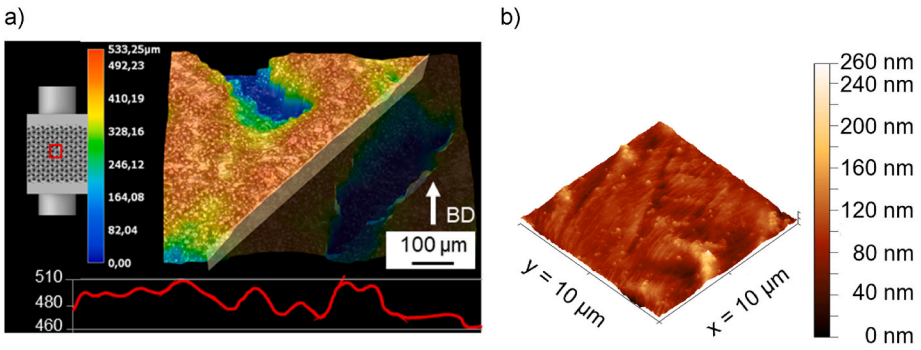

Fig. 10. a) Macro-roughness of lattice structure struts and b) nano-topology between unmelted powder particles of AM Ti–6Al–4V using atomic force microscopy (AFM).

Additionally, multiple crack initiation spots were identified, likely driven by the increased surface roughness caused by the manufacturing process. This roughness, combined with an amplified notch factor effect at various critical locations, further promotes crack formation. These results of the fractographic investigations led to further characterization of the surface roughness of additively manufactured TPMS lattice structures on macro- and micro-scales. Focusing on the macro-surface roughness shown in Fig. 10a, homogenous but comparatively high values between 460 and 510 µm can be detected on the struts of the lattice which highly promote and cause failure during cyclic loading as shown in Fig. 9. Additionally, the micro-roughness was characterized using atomic force microscopy in between unmelted powder particles. Results of the topography signal show homogenous and comparatively low micro-roughness of approx. 120 nm and support the assumption, that crack initiation must be caused by comparatively high macro-roughness [22,45].

These findings highlight the complex interaction between surface properties, geometrical factors, and material properties which affect the fatigue performance of additively manufactured Ti–6Al–4V lattice structures.

4. Conclusions

Correlating all results of this study about the mechanical characterization of additively manufactured Ti–6Al–4V lattice structures, the main findings of the quasistatic properties, the fatigue behavior, and damage evolution are summarized below including important microstructural effects that help to improve the understanding of damage mechanisms in complex lattice structures:

Increased cavities (reduced density of 70 %) of complex lattice structures lead to adapted stiffness of around 30 GPa and mechanical properties (reduced fatigue life) compared to bulk material for medical implant applications and reduce the phenomena of stress shielding.

Density-related fatigue behavior was identified with small deviations inside the S–N curve which leads to a good correlation with the Basquin equation but need to take further properties into account in order to archive local stress concentrations of complex structures.

Damage mechanisms and damage evolution of lattices are complex and require suitable measurement techniques for detection, such as high-resolution digital image correlation (DIC) and the potential drop method for enhanced damage description and crack detection at specimen surface.

Enhanced surface roughness characterization methods using AFM show micro surface roughness between 100 and 120 nm for the powder particle-free areas which is important for further biological investigations and coatings. Optical microscopy and fractographic analysis (SEM) show that macro-roughness affects the fatigue lifetime and crack initiation processes of lattice structures. While critical manufacturing-related defects (microporosity) often cause fatigue failure of bulk material, for lattice structures surface roughness and notch factor effects of the geometrical design are more critical for fatigue lifetime and need to be considered.

Declaration of competing interest

The authors declare that they have no known competing financial interests or personal relationships that could have appeared to influence the work reported in this paper.

Acknowledgments

The authors thank the German Research Foundation (DFG) for its financial support within subproject 3 of the research unit FOR 5250 “Mechanism-based characterization and modeling of permanent and bioresorbable implants with tailored functionality based on innovative in vivo, in vitro and in silico methods” (project no. 449916462) and the Ministry of Culture and Science of North Rhine-Westphalia for their financial support within the Major Research Instrumentation Program for the CT-system Procon Alpha-Duo (project no. 459685720) and the In situ atomic force microscope (project no. 445052562).

The authors would also like to thank the Laser Center Hannover e.V. for manufacturing the specimens and all project partners within the research unit 5250, “Mechanism-based characterization and modeling of permanent and bioresorbable implants with tailored functionality based on innovative in vivo, in vitro and in silico methods,” for the excellent scientific collaboration.

Further, the authors thank the German Federal Ministry for Economic Affairs and Climate Action (BMWK), managed by AiF Projekt GmbH within Central Innovation Program for SMEs (ZIM), for the funding of the project “Development of a test rig for the short-term characterization of long-term fatigue properties (load cycles >100 million) of hybrid structures using 3D high-speed deformation and hysteresis monitoring” (KK5072223AB2).

References

[1] Shibo G, Xuanhui Q, Xinbo H, Ting Z, Bohua D. Powder injection molding of Ti–6Al–4V alloy. J Mater Process Technol 2006;173:310–4. https://doi.org/10.1016/j.jmatprotec.2005.12.001.

[2] Niinomi M, Nakai M, Hieda J. Development of new metallic alloys for biomedical applications. Acta Biomater 2012;8:3888–903. https://doi.org/10.1016/j.actbio.2012.06.037.

[3] Golasiński KM, Detsch R, Szklarska M, Łosiewicz B, Zubko M, Mackiewicz S, Pieczyska EA, Boccaccini AR. Evaluation of mechanical properties, in vitro corrosion resistance and biocompatibility of Gum Metal in the context of implant applications. Journal of the mechanical behavior of biomedical materials 2021;115:104289. https://doi.org/10.1016/j.jmbbm.2020.104289.

[4] Sidambe AT. Biocompatibility of advanced manufactured titanium implants-A review. Materials 2014;7:8168–88. https://doi.org/10.3390/ma7128168.

[5] Nikiel P, Wróbel M, Szczepanik S, Stępień M, Wierzbanowski K, Baczmański A. Microstructure and mechanical properties of Titanium grade 23 produced by selective laser melting. Arch Civ Mech Eng 2021;21. https://doi.org/10.1007/s43452-021-00304-5.

[6] Tang HP, Zhao P, Xiang CS, Liu N, Jia L. Ti-6Al-4V orthopedic implants made by selective electron beam melting. In: Froes FH, Qian M, editors. Titanium in medical and dental applications. Kidlington, Cambridge, MA, Duxford: Woodhead Publishing an imprint of Elsevier; 2018. p. 239–49.
[7] Yadroitsev I, Krakhmalev P, Yadroitsava I, Du Plessis A. Qualification of Ti6Al4V ELI alloy produced by laser powder bed fusion for biomedical applications. JOM 2018;70:372–7. https://doi.org/10.1007/s11837-017-2655-5.
[8] Ridzwan M, Shuib S, Hassan AY, Shokri AA, Mohamad Ib MN. Problem of Stress Shielding and improvement to the hip implant designs: a review. J. of Medical Sciences 2007;7:460–7. https://doi.org/10.3923/jms.2007.460.467.
[9] Noyama Y, Miura T, Ishimoto T, Itaya T, Niinomi M, Nakano T. Bone loss and reduced bone quality of the human femur after total hip arthroplasty under Stress-Shielding effects by titanium-based implant. Mater Trans 2012;53:565–70. https://doi.org/10.2320/matertrans.M2011358.
[10] Al-Ketan O, Lee D-W, Rowshan R, Abu Al-Rub RK. Functionally graded and multi-morphology sheet TPMS lattices: design, manufacturing, and mechanical properties. Journal of the mechanical behavior of biomedical materials 2020;102:103520. https://doi.org/10.1016/j.jmbbm.2019.103520.
[11] Wang N, Meenashisundaram GK, Kandilya D, Fuh JYH, Dheen ST, Kumar AS. A biomechanical evaluation on Cubic, Octet, and TPMS gyroid Ti6Al4V lattice structures fabricated by selective laser melting and the effects of their debris on human osteoblast-like cells. Biomaterials advances 2022;137:212829. https://doi.org/10.1016/j.bioadv.2022.212829.
[12] Markhoff J, Krogull M, Schulze C, Rotsch C, Hunger S, Bader R. Biocompatibility and inflammatory potential of titanium alloys cultivated with human osteoblasts, fibroblasts and macrophages. Materials 2017;10:52. https://doi.org/10.3390/ma10010052.
[13] Araya M, Jaskari M, Rautio T, Guillén T, Järvenpää A. Assessing the compressive and tensile properties of TPMS-Gyroid and stochastic Ti64 lattice structures: a study on laser powder bed fusion manufacturing for biomedical implants. J Sci: Advanced Materials and Devices 2024;9:100663. https://doi.org/10.1016/j.jsamd.2023.100663.
[14] Naghavi SA, Tamaddon M, Marghoub A, Wang K, Babamiri BB, Hazeli K, Xu W, Lu X, Sun C, Wang L, Moazen M, Wang L, Li D, Liu C. Mechanical characterisation and numerical modelling of TPMS-based gyroid and diamond Ti6Al4V scaffolds for bone implants: an integrated approach for translational consideration, vol. 9. Bioengineering (Basel, Switzerland); 2022. https://doi.org/10.3390/bioengineering9100504.
[15] Stammkötter S, Teschke M, Mrzljak S, Koch A, Walther F. Assessing the performance and damage evolution of additively manufactured structures. In: Krupp U, editor. Tagungsband Werkstoffprüfung; 2024, 2024. p. 205–10.
[16] Stammkötter S, Walther F. Evaluation of the damage evolution of additive-manufactured TPMS lattice structures for medical implants. In: Krupp U, editor. Tagungsband Werkstoffprüfung; 2024, 2024. p. 211–6.
[17] Hitchon S, Anderson W, Milner JS, Hong G, Ivanov T, Willing R, Holdsworth D. Static compression and fatigue behavior of heat-treated selective laser melted titanium alloy (Ti6Al4V) gyroid cylinders. Journal of the mechanical behavior of biomedical materials 2023;146:106076. https://doi.org/10.1016/j.jmbbm.2023.106076.
[18] Sathishkumar N, Arunkumar N, Rohith SV, Hariharan RR. Effect of varying unit cell size on energy absorption behaviour of additive manufactured TPMS PETG lattice structure. Progress in Additive Manufacturing 2023;8:1379–91. https://doi.org/10.1007/s40964-023-00407-w.
[19] Zhou H, Zhao M, He N, Zhang T, Ma X, Zhang DZ. Compressive response and energy absorption of additive manufactured Ti-6Al-4V triply periodic minimal surface honeycomb structure. J Alloys Compd 2024;982:173744. https://doi.org/10.1016/j.jallcom.2024.173744.
[20] Sun Q, Sun J, Guo K, Wang L. Compressive mechanical properties and energy absorption characteristics of SLM fabricated Ti6Al4V triply periodic minimal surface cellular structures. Mech Mater 2022;166:104241. https://doi.org/10.1016/j.mechmat.2022.104241.
[21] Tjandra J, Alabort E, Barba D, Pedrazzini S. Corrosion, fatigue and wear of additively manufactured Ti alloys for orthopaedic implants. Mater Sci Technol 2023;39:2951–65. https://doi.org/10.1080/02670836.2023.2230417.
[22] Yánez A, Fiorucci MP, Cuadrado A, Martel O, Monopoli D. Surface roughness effects on the fatigue behaviour of gyroid cellular structures obtained by additive manufacturing. Int J Fatig 2020;138:105702. https://doi.org/10.1016/j.ijfatigue.2020.105702.
[23] Pirotais M, Saintier N, Brugger C, Conesa V. Ti-6Al-4V lattices obtained by SLM: characterisation of the heterogeneous high cycle fatigue behaviour of thin walls. Procedia Struct Integr 2022;38:132–40. https://doi.org/10.1016/j.prostr.2022.03.014.
[24] Liu Z, Gong H, Gao J. Enhancement in the fatigue resistances of triply periodic surfaces-based scaffolds. Int J Mech Sci 2023;245:108119. https://doi.org/10.1016/j.ijmecsci.2023.108119.
[25] Kotzem D, Arold T, Bleicher K, Raveendran R, Niendorf T, Walther F. Ti6Al4V lattice structures manufactured by electron beam powder bed fusion - microstructural and mechanical characterization based on advanced in situ techniques. J Mater Res Technol 2023;22:2111–30. https://doi.org/10.1016/j.jmrt.2022.12.075.
[26] Kotzem D, Walther F. Mechanical assessment of PBF-EB manufactured IN718 lattice structures. In: Da Silva LFM, Ravi Kumar D, Reis Vaz MdF, Carbas RJC, editors. 1st international Conference on engineering Manufacture 2022. Cham: Springer International Publishing; 2023. p. 3–18.
[27] Park M, Venter MP, Du Plessis A. Assessing the impact of process parameters on lattice structure manufacturing defects through micro-CT scanning. MATEC Web Conf. 2023;388:8005. https://doi.org/10.1051/matecconf/202338808005.
[28] Bidulský R, Bidulská J, Gobber FS, Kvačkaj T, Petroušek P, Actis-Grande M, Weiss K-P, Manfredi D. Case study of the tensile fracture investigation of additive manufactured austenitic stainless steels treated at cryogenic conditions. Materials 2020;13. https://doi.org/10.3390/ma13153328.
[29] Bidulská J, Bidulský R, Actis Grande M, Kvačkaj T. Different Formation routes of pore structure in aluminum powder metallurgy alloy. Materials 2019;12. https://doi.org/10.3390/ma12223724.
[30] Rezapourian M, Jasiuk I, Saarna M, Hussainova I. Selective laser melted Ti6Al4V split-P TPMS lattices for bone tissue engineering. Int J Mech Sci 2023;251:108353. https://doi.org/10.1016/j.ijmecsci.2023.108353.
[31] Yan C, Hao L, Hussein A, Wei Q, Shi Y. Microstructural and surface modifications and hydroxyapatite coating of Ti-6Al-4V triply periodic minimal surface lattices fabricated by selective laser melting. Mater Sci Eng C 2017;75:1515–24. https://doi.org/10.1016/j.msec.2017.03.066.
[32] Mrzljak S, Trautmann M, Blickling P, Wagner G, Walther F. Fatigue condition monitoring of notched thermoplastic-based hybrid fiber metal laminates using electrical resistance measurement and digital image correlation. J Compos Mater 2023;57:2669–87. https://doi.org/10.1177/00219983231176257.
[33] Mrzljak S, Trautmann M, Wagner G, Walther F. Very high cycle fatigue assessment of thermoplastic-based hybrid fiber metal laminate by using a high-frequency resonant testing system. Int J Fatig 2024;186:108361. https://doi.org/10.1016/j.ijfatigue.2024.108361.
[34] Khorasani A, Gibson I, Awan US, Ghaderi A. The effect of SLM process parameters on density, hardness, tensile strength and surface quality of Ti-6Al-4V. Addit Manuf 2019;25:176–86. https://doi.org/10.1016/j.addma.2018.09.002.
[35] Lekoadi P, Tlotleng M, Annan K, Maledi N, Masina B. Evaluation of heat treatment parameters on microstructure and hardness properties of high-speed selective laser melted Ti6Al4V. Metals 2021;11:255. https://doi.org/10.3390/met11020255.
[36] Stammkötter S, Tenkamp J, Teschke M, Donnerbauer K, Koch A, Platt T, Biermann D, Walther F. Fatigue and short crack assessment of powder bed fusion laser-based fabricated AlSi10Mg miniature specimens under alternating bending load. Mater Des 2024;247:113412. https://doi.org/10.1016/j.matdes.2024.113412.
[37] Fotovvati B, Namdari N, Dehghanghadikolaei A. Fatigue performance of selective laser melted Ti6Al4V components: state of the art. Mater Res Express 2019;6:12002. https://doi.org/10.1088/2053-1591/aae10e.
[38] Dallago M, Fontanari V, Torresani E, Leoni M, Pederzolli C, Potrich C, Benedetti M. Fatigue and biological properties of Ti-6Al-4V ELI cellular structures with variously arranged cubic cells made by selective laser melting. Journal of the mechanical behavior of biomedical materials 2018;78:381–94. https://doi.org/10.1016/j.jmbbm.2017.11.044.
[39] Beiss P, Dalgic M. Structure property relationships in porous sintered steels. Mater Chem Phys 2001;67:37–42. https://doi.org/10.1016/S0254-0584(00)00417-X.
[40] Etesami SA, Fotovvati B, Asadi E. Heat treatment of Ti-6Al-4V alloy manufactured by laser-based powder-bed fusion: process, microstructures, and mechanical properties correlations. J Alloys Compd 2022;895:162618. https://doi.org/10.1016/j.jallcom.2021.162618.
[41] Niinomi M, Nakai M. Titanium-based biomaterials for preventing stress shielding between implant devices and bone. International journal of biomaterials 2011;2011:836587. https://doi.org/10.1155/2011/836587.
[42] Koju N, Niraula S, Fotovvati B. Additively manufactured porous Ti6Al4V for bone implants: A review. Metals 2022;12:687. https://doi.org/10.3390/met12040687.
[43] Timercan A, Terriault P, Brailovski V. Axial tension/compression and torsional loading of diamond and gyroid lattice structures for biomedical implants: Simulation and experiment. Mater Des 2023;225:111585. https://doi.org/10.1016/j.matdes.2022.111585.
[44] Gandhi R, Pagliari L, Gerosa R, Concli F. Quasi-static and fatigue performance of Ti-6Al-4V triply periodic minimal surface scaffolds manufactured via laser powder bed fusion for hard-tissue engineering. Results in Engineering 2024;24:103101. https://doi.org/10.1016/j.rineng.2024.103101.
[45] Nakatani M, Masuo H, Tanaka Y, Murakami Y. Effect of surface roughness on fatigue strength of Ti-6Al-4V alloy manufactured by additive manufacturing. Procedia Struct Integr 2019;19:294–301. https://doi.org/10.1016/j.prostr.2019.12.032.